Title

Multiharmonic small-signal modeling of low-power PWM dc-dc converters

Authors

Wang, Ya
Gao, Di
Tannir, Dani
et al.

Publication Date

2017

Peer reviewed

Multiharmonic Small-Signal Modeling of Low-Power PWM DC-DC Converters

YA WANG, Texas A&M University
DI GAO, Cadence Design Systems Inc.
DANI TANNIR, Lebanese American University
NING DONG, G. PETER FANG, and WEI DONG, Texas Instruments Inc.
PENG LI, Texas A&M University

Small-signal models of pulse-width modulation (PWM) converters are widely used for analyzing stability and play an important role in converter design and control. However, existing small-signal models either are based on averaged DC behaviors, and hence are unable to capture frequency responses that are faster than the switching frequency, or greatly approximate these high-frequency responses. We address the severe limitations of the existing models by proposing a multiharmonic model that provides a complete small-signal characterization of both DC averages and high-order harmonic responses. The proposed model captures important high-frequency overshoots and undershoots of the converter response, which are otherwise unaccounted for by the existing techniques. In two converter examples, the proposed model corrects the misleading results of the existing models by providing truthful characterization of the overall converter AC response and offers important guidance for converter design and closed-loop control.

CCS Concepts: • **Computing methodologies** → **Modeling and simulation**; • **Hardware** → Electronic design automation;

Additional Key Words and Phrases: Integrated circuit modeling, multiharmonic averaging, switched mode power supplies, DC-DC converters

ACM Reference Format:
Ya Wang, Di Gao, Dani Tannir, Ning Dong, G. Peter Fang, Wei Dong, and Peng Li. 2017. Multiharmonic small-signal modeling of low-power PWM DC-DC converters. ACM Trans. Des. Autom. Electron. Syst. 22, 4, Article 68 (June 2017), 16 pages.
DOI: http://dx.doi.org/10.1145/3057274

1. INTRODUCTION

For the efficient Electronic Design Automation (EDA) of power management and distribution circuits, there is an increasing need for accurate control techniques for the design and simulation of Pulse-Width Modulation (PWM) DC-DC converters in modern low-power integrated circuits [Zeng et al. 2013]. Converter circuit behavior is typically

This work is supported by the National Science Foundation (grant no. CCF-1117660) and by the Semiconductor Research Corporation through the Texas Analog Center of Excellence at the University of Texas at Dallas (Task ID:1836.115). This publication was also made possible by NPRP grant no. NPRP 8-274-2-107 from the Qatar National Research Fund (a member of the Qatar Foundation). The statements made herein are solely the responsibility of the authors.
Authors' addresses: D. Tannir, Electrical and Computer Engineering Department, Lebanese American University, P.O. Box 36, Byblos, Lebanon; email: dani.tannir@lau.edu.lb; Y. Wang and P. Li, Electrical and Computer Engineering Department, Texas A&M University, College Station, TX 77843, USA; emails: {tonywang, pli}@tamu.edu; D. Gao, Cadence Design Systems Inc., San Jose, CA, USA; email: dgao63@hotmail.com; N. Dong, G. P. Fang, and W. Dong, Texas Instruments Inc., Dallas, TX 75266, USA; emails: {ningd, gfang1, weidong}@ti.com.

DOI: http://dx.doi.org/10.1145/3057274

highly nonlinear due to the strong switching activities and the presence of nonlinear devices. The small-signal model, which approximates the behavior of the DC-DC converter by linearizing the nonlinear devices and switches at a certain DC operating point, is widely used by designers to design the control blocks and closed-loop systems, as well as to analyze system stability.

Typically, a small-signal model is obtained by first deriving the averaged model of the DC-DC converter, then injecting perturbations to the averaged model through the control signal/supply voltage, followed by evaluating the sensitivity of the circuit states. Thus, the accuracy of the small-signal model relies on the accuracy of the averaged models, which depend on one of several different existing DC-DC converter averaging techniques. The circuit averaging technique first introduced in Wester and Middlebrook [1973] and Vorperian [1990] constructs the small-signal model based on the averaged models of linearized switch cells. This method is extended in Vorpérian [1990], where DC-DC converters operating in the discontinuous conduction mode (DCM) are also considered. The sampled-data modeling approach introduced in Verghese et al. [1986] and Shortt and Lee [1982] builds linear discrete small-signal models with consideration of the time-variant discrete nature of DC-DC converters. The state-space averaging technique introduced in Sun et al. [2001] uses a set of differential equations to represent the averaged model of DC-DC converters with a modification matrix that takes the DCM operation into account, which is further developed into small-signal models that are applicable to both DCM and continuous conduction mode (CCM) operations. Alternatively, the approaches in Noworolski and Sanders [1991] and Sanders et al. [1991] present generalized averaged models with harmonic components considered, from which a condensed approximate second-order small-signal model is developed, which in turn considers the interaction of the harmonic components with the DC averages [Caliskan et al. 1999].

Unfortunately, since the state-space averaging process eliminates the inherent sampling nature of the switching converter, the accuracy of the average model is questionable at frequencies approaching half that of the switching frequency [Qiu et al. 2006]. Therefore, none of these existing works have made successful attempts to fully capture the harmonic components while constructing the small-signal model, and none of these models can accurately capture circuit responses faster than the switching frequency. For low-power DC-DC converters, it is critically important to capture the high-frequency circuit responses in stability analysis and closed-loop design. For example, Scandola et al. [2015] demonstrate significant accuracy improvement in small-signal models by capturing high-order harmonics in DC-DC series resonant converters. Alternatively, harmonic balance-based approaches have been proposed for small-signal modeling [Groves 1991; Feldmann and Roychowdhury 1996]. Harmonic balance-based small-signal analysis solves the periodic steady states at multiple harmonics and linearizes the system at multiple harmonics, thereby generating periodically time-varying transfer functions. Although such techniques do allow for accurate behavior prediction at relatively high frequencies, they are not an efficient means for extracting physical design insights out of the complicated model [Qiu et al. 2006].

Recently, an enhanced circuit averaged model for PWM DC-DC converters was introduced to accurately account for the effects of device nonidealities in low-power integrated circuits [Tannir et al. 2016]. The method in Tannir et al. [2016] was, however, limited to modeling the DC-level behavioral effects of the converter. In Wang et al. [2016], a multiharmonic large-signal model was first introduced to efficiently model the higher-order effects of the converter behavior while also accounting for the effects of device nonidealities when performing time-domain simulations. In this article, we present for the first time a multiharmonic small-signal model that demonstrates significant accuracy improvements in high-frequency responses over existing methods in

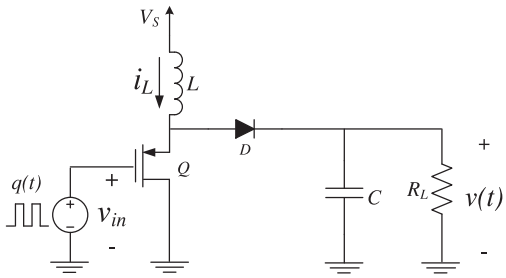

Fig. 1. A boost converter.

the literature, thereby providing useful design insights for critical applications such as optimization and design centering. The focus of this article is therefore on presenting an efficient and accurate model for the analysis and design of low-power PWM converters. We first derive a multiharmonic averaged model, which is a six-state variable system that considers both the DC response and the first-order harmonics as well as the interactions between them. We then develop a small-signal model to accurately capture the small-signal dependencies of each harmonic component on the targeted input perturbation. The proposed model is presented in both the state-space form and the frequency domain. We compare the proposed small-signal model with the conventional small-signal model, which is based on the average model that only considers the DC component of the Fourier series of the signals [Erickson and Maksimovic 2007], in two converter examples to demonstrate the significant accuracy enhancement that is offered by using the proposed model in high-frequency circuit responses. We will show that the proposed model has a time-varying aspect and has the ability to identify misleading results that can result from using conventional small-signal models. The proposed model therefore provides the actual behavior of the converters that will in turn lead to stable closed-loop designs.

This article is organized as follows. Following this introduction, Section 2 presents an overview of the derivation for the large-signal multiharmonic average model. Section 3 then presents the derivation of the small-signal state-space model, while Section 4 shows how we cast the small-signal state-space model to the frequency domain to derive a linear time-varying AC model that can capture important high-frequency characteristics and lead to useful design insights. Experimental results to demonstrate the improved accuracy of the proposed model are in Section 5, followed by the conclusion in the final section.

2. MULTIHARMONIC AVERAGE MODEL

In this section, we present an overview of the derivation for the large-signal multiharmonic average model. The multiharmonic average model takes both the DC average and the multiple harmonic components into account [Caliskan et al. 1999]. Note that while the derivation will be based on the standard boost converter shown in Figure 1, fundamentally similar derivations can be applied to other PWM DC-DC converter topologies, including buck- and buck-boost-type converters [Wang et al. 2016; Tannir et al. 2016].

We begin the derivation with the equations that describe the switched model of the boost converter operating in CCM and controlled by the switching function $q(t)$:

$$\frac{di(t)}{dt} = \frac{1}{L}(V_S - (1 - q(t))v(t)) \tag{1}$$

$$\frac{dv(t)}{dt} = \frac{1}{C}\left((1-q(t))i(t) - \frac{1}{R}v(t)\right). \tag{2}$$

The switching function is binary and can be expressed as

$$q(t) = \begin{cases} 1 & t \in (0, dT_s) \quad \text{switch is ON} \\ 0 & t \in (dT_s, T_s) \quad \text{switch is OFF,} \end{cases} \tag{3}$$

where d is the duty ratio of the switching function and T_s is the switching period. We capture the variation of each state variable $x(\tau)$ (i.e., v and i in Equation (1)) within each switching cycle by decomposing it into a Fourier series with time-varying coefficients as

$$x(\tau) = \sum_{k=-\infty}^{\infty} \langle x\rangle_k(t) e^{jk\omega_s\tau}, \tag{4}$$

where $\omega_s = 2\pi f_s$ and f_s is the switching frequency. $\langle x\rangle_k(t)$ is the k^{th} complex Fourier coefficient [Sanders et al. 1991], which is given by

$$\langle x\rangle_k(t) = \frac{1}{T_s}\int_{t-T_s}^{t} x(\tau)e^{-jk\omega_s\tau}d\tau. \tag{5}$$

From Equation (5), it is clear that the k^{th} complex Fourier coefficient of a state variable in Equation (1) is in fact its average value at the frequency kf_s. Thus, we refer to the k^{th} complex Fourier coefficient $\langle x\rangle_k(t)$ as the index-k average.

Going forward, we will develop the proposed small-signal model using only the index-0 and index-1 terms in the derivation as we believe they will present sufficient accuracy for most practical applications while still having the important ability to obtain design insights from the model that are critically important for low-power converter design, such as performing a stability analysis. It is important to note here that the developed models can be augmented by including higher orders of index-k averages when necessary. This would result in a multiharmonic model that approximates the nonlinear behavior of the switch model more accurately, but at the cost of increased complexity. However, the fact that index-1 averages correspond to the most significant fundamental harmonics implies it is sufficient to only have index-0 and index-1 components for most practical cases of DC-DC converters, which are not typically used as conventional analog circuits. This is more clearly illustrated in Figure 2, which shows the FFT spectrum of the output voltage of a standard boost converter operating in the steady state. As can be seen, the magnitudes of the index-0 and the index-1 components are measured to be $18dB$ and $-40dB$, respectively, which dominate the overall circuit response. In comparison, the magnitudes of all the other higher-order harmonic components are less than $-60dB$, which is no more than 4% of the magnitude of the index-1 component, thus confirming our original assumption that by including the index-0 and the index-1 components, the multiharmonic model is able to capture the circuit behavior with sufficient accuracy. This will also be verified in the results of the numerical examples in Section 5.

To calculate the index-0 averages, we need to apply the discrete convolution and conjugation property to Equation (1). According to Caliskan et al. [1999], we have

$$\frac{d\langle i\rangle_0}{dt} = \frac{1}{L}\big(-\langle q'\rangle_0\langle v\rangle_0 + 2\big(\langle q\rangle_1^R\langle v\rangle_1^R + \langle q\rangle_1^I\langle v\rangle_1^I\big)\big) \tag{6}$$

$$\frac{d\langle v\rangle_0}{dt} = \frac{1}{C}\left(\langle q'\rangle_0\langle i\rangle_0 - \frac{\langle v\rangle_0}{R} - 2\big(\langle q\rangle_1^R\langle i\rangle_1^R + \langle q\rangle_1^I\langle i\rangle_1^I\big)\right), \tag{7}$$

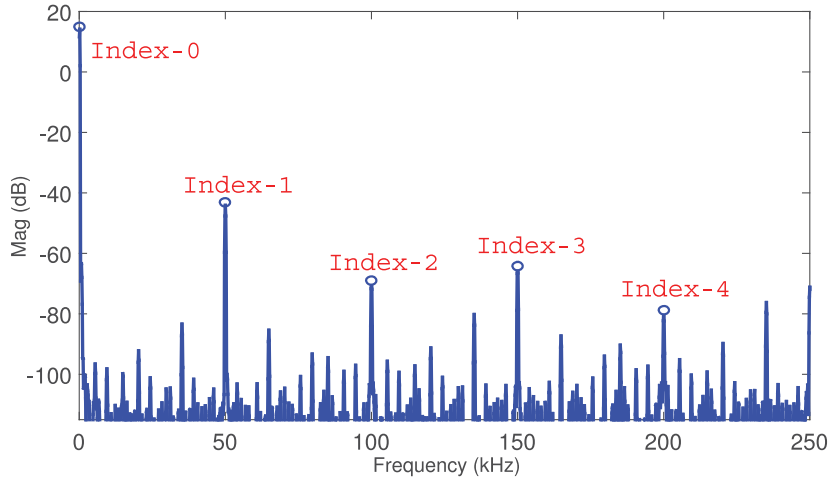

Fig. 2. The FFT spectrum of the output voltage of a boost converter operating in the steady state.

where $q' = 1 - q$, $\langle\cdot\rangle_1^R$ and $\langle\cdot\rangle_1^I$ are the real part and imaginary part of the index-1 average $\langle\cdot\rangle_1$. Similarly, the index-1 average of the switch model (Equation (1)) can be calculated as

$$\frac{d\langle i\rangle_1^R}{dt} = \omega_s\langle i\rangle_1^I + \frac{1}{L}\left(-\langle q'\rangle_0\langle v\rangle_1^R + \langle v\rangle_0\langle q\rangle_1^R\right) \tag{8}$$

$$\frac{d\langle v\rangle_1^R}{dt} = \omega_s\langle v\rangle_1^I + \frac{1}{C}\left(\langle q'\rangle_0\langle i\rangle_1^R - \langle i\rangle_0\langle q\rangle_1^R - \frac{\langle v\rangle_1^R}{R}\right) \tag{9}$$

$$\frac{d\langle i\rangle_1^I}{dt} = -\omega_s\langle i\rangle_1^R + \frac{1}{L}\left(-\langle q'\rangle_0\langle v\rangle_1^I + \langle v\rangle_0\langle q\rangle_1^I\right) \tag{10}$$

$$\frac{d\langle v\rangle_1^I}{dt} = -\omega_s\langle v\rangle_1^R + \frac{1}{C}\left(\langle q'\rangle_0\langle i\rangle_1^I - \langle i\rangle_0\langle q\rangle_1^I - \frac{\langle v\rangle_1^I}{R}\right). \tag{11}$$

Now we have a highly coupled system of two state variables of index-0 and four state variables of index-1, which define the dynamic behavior of the boost converter. Notice that Equations (6) through (11) rely on the index-0 and index-1 averages of the switching function $q(t)$. Substituting Equation (3) into Equation (5) gives the relation of the index-0 and index-1 averages of the switching function to the duty ratio d as

$$\langle q\rangle_0 = d \tag{12}$$

$$\langle q\rangle_1^R = \frac{1}{2\pi}sin(\omega_s t + 2\pi d) \tag{13}$$

$$\langle q\rangle_1^I = \frac{1}{2\pi}\left[cos(\omega_s t + 2\pi d) - 1\right]. \tag{14}$$

Finally, by combining Equations (6) and (7) with Equations (8) to (11) and Equations (12) to (14), the final multiharmonic averaged model of the boost converter including index-0 and index-1 averages is specified.

3. SMALL-SIGNAL STATE-SPACE MODEL

The small-signal model characterizes the sensitivities of the circuit state variables to the perturbation of parameters such as duty ratio or supply voltage. In this article, we

will focus on the perturbation of the duty ratio. Let us assume that the boost converter is in steady state and there is a perturbation in the duty ratio of the form

$$d = \bar{d} + \hat{d}, \tag{15}$$

where $\bar{d}$ is the steady-state value of the duty ratio and $\hat{d}$ is the small-signal perturbation. The immediate effect of the duty ratio perturbation is the variation of switching functions. Based on the relations given by Equations (12) through (15), the variations of the index-0 and index-1 averages of the switching function are

$$\langle \hat{q} \rangle_0 = \hat{d} \tag{16}$$

$$\langle \hat{q} \rangle_1^R = \frac{1}{2\pi} \left[sin\left(\omega_s t + 2\pi(\bar{d} + \hat{d})\right) - sin(\omega_s t + 2\pi\bar{d}) \right] \tag{17}$$

$$\langle \hat{q} \rangle_1^I = \frac{1}{2\pi} \left[cos\left(\omega_s t + 2\pi(\bar{d} + \hat{d})\right) - cos(\omega_s t + 2\pi\bar{d}) \right], \tag{18}$$

in which $\langle \hat{q} \rangle_1^R$ and $\langle \hat{q} \rangle_1^I$ are nonlinear functions of the duty ratio perturbation $\hat{d}$. Next, we linearize Equations (16) through (18) around $d = \bar{d}$ as $[\ \langle \hat{q} \rangle_0\ \ \langle \hat{q} \rangle_1^R\ \ \langle \hat{q} \rangle_1^I\ ]^T = Q_s \cdot \hat{d}$, where

$$Q_s = \begin{bmatrix} 1 \\ cos\left(\omega_s t + 2\pi\bar{d}\right) \\ -sin\left(\omega_s t + 2\pi\bar{d}\right) \end{bmatrix} \tag{19}$$

is the switching function input matrix.

The effect of the perturbation continues to propagate to each of the state variables. Based on Equations (6) and (7), the perturbation of index-0 state variables can be calculated as

$$\begin{aligned} \frac{d\langle \hat{i} \rangle_0}{dt} &= \frac{1}{L}\left((\langle \bar{q} \rangle_0 - 1)\langle \hat{v} \rangle_0 + \langle \bar{v} \rangle_0 \langle \hat{q} \rangle_0 \right) + \frac{2}{L}\left(\langle \bar{q} \rangle_1^R \langle \hat{v} \rangle_1^R + \langle \bar{v} \rangle_1^R \langle \hat{q} \rangle_1^R \right) \\ &\quad + \frac{2}{L}\left(\langle \bar{q} \rangle_1^I \langle \hat{v} \rangle_1^I + \langle \bar{v} \rangle_1^I \langle \hat{q} \rangle_1^I \right) \end{aligned} \tag{20}$$

$$\begin{aligned} \frac{d\langle \hat{v} \rangle_0}{dt} &= \frac{1}{C}\left((1 - \langle \bar{q} \rangle_0)\langle \hat{i} \rangle_0 + \langle \bar{i} \rangle_0 \langle \hat{q} \rangle_0 - \frac{\langle \hat{v} \rangle_0}{R} \right) - \frac{2}{C}\left(\langle \bar{q} \rangle_1^R \langle \hat{i} \rangle_1^R + \langle \bar{i} \rangle_1^R \langle \hat{q} \rangle_1^R \right) \\ &\quad - \frac{2}{C}\left(\langle \bar{q} \rangle_1^I \langle \hat{i} \rangle_1^I + \langle \bar{i} \rangle_1^I \langle \hat{q} \rangle_1^I \right). \end{aligned} \tag{21}$$

Similarly, the perturbation of the index-1 state variables can be calculated as

$$\frac{d\langle \hat{i} \rangle_1^R}{dt} = \omega_s \langle \hat{i} \rangle_1^I + \frac{1}{L}\left(-\langle \hat{v} \rangle_1^R + \langle \bar{q} \rangle_0 \langle \hat{v} \rangle_1^R + \langle \bar{v} \rangle_1^R \langle \hat{q} \rangle_0 + \langle \bar{q} \rangle_1^R \langle \hat{v} \rangle_0 + \langle \bar{v} \rangle_0 \langle \hat{q} \rangle_1^R \right) \tag{22}$$

$$\frac{d\langle \hat{v} \rangle_1^R}{dt} = \omega_s \langle \hat{v} \rangle_1^I + \frac{1}{C}\left(\langle \hat{i} \rangle_1^R - \frac{\langle \hat{v} \rangle_1^R}{R} - \langle \bar{q} \rangle_0 \langle \hat{i} \rangle_1^R - \langle \bar{i} \rangle_1^R \langle \hat{q} \rangle_0 - \langle \bar{q} \rangle_1^R \langle \hat{i} \rangle_0 + \langle \bar{i} \rangle_0 \langle \hat{q} \rangle_1^R \right) \tag{23}$$

$$\frac{d\langle \hat{i} \rangle_1^I}{dt} = -\omega_s \langle \hat{i} \rangle_1^R + \frac{1}{L}\left(-\langle \hat{v} \rangle_1^I + \langle \bar{q} \rangle_0 \langle \hat{v} \rangle_1^I + \langle \bar{v} \rangle_1^I \langle \hat{q} \rangle_0 + \langle \bar{q} \rangle_1^I \langle \hat{v} \rangle_0 + \langle \bar{v} \rangle_0 \langle \hat{q} \rangle_1^I \right) \tag{24}$$

$$\frac{d\langle \hat{v} \rangle_1^I}{dt} = -\omega_s \langle \hat{v} \rangle_1^R + \frac{1}{C}\left(\langle \hat{i} \rangle_1^I - \frac{\langle \hat{v} \rangle_1^I}{R} - \langle \bar{q} \rangle_0 \langle \hat{i} \rangle_1^I - \langle \bar{i} \rangle_1^I \langle \hat{q} \rangle_0 - \langle \bar{q} \rangle_1^I \langle \hat{i} \rangle_0 + \langle \bar{i} \rangle_0 \langle \hat{q} \rangle_1^I \right). \tag{25}$$

Combining Equations (20) and (21) with Equations (22) through (25) and rewriting the equations into a state-space representation gives

$$\frac{d}{dt}\begin{bmatrix} \langle \vec{x} \rangle_0 \\ \langle \vec{x} \rangle_1 \end{bmatrix} = \begin{bmatrix} A_1 & A_2 \\ A_3 & A_4 \end{bmatrix} \begin{bmatrix} \langle \vec{x} \rangle_0 \\ \langle \vec{x} \rangle_1 \end{bmatrix} + \begin{bmatrix} B_1 \\ B_2 \end{bmatrix} \cdot Q_s \cdot \hat{d}, \tag{26}$$

where $\langle \vec{x} \rangle_0 = [\langle i \rangle_0 \ \langle v \rangle_0]^T$ is the vector of index-0 state variables and $\langle \vec{x} \rangle_1 = [\langle \hat{i} \rangle_1^R \ \langle \hat{v} \rangle_1^R \ \langle \hat{i} \rangle_1^I \ \langle \hat{v} \rangle_1^I]^T$ is the vector of index-1 state variables. The state matrix A and input matrix B are partitioned to form two subsystems. A_1 and A_4 represent the subsystems of the index-0 components and index-1 components. A_2 and A_3 represent the interaction between those two subsystems. Similarly, B_1 and B_2 represent the input to the index-0 and index-1 subsystems. The submatrices in state matrix A and the input matrix B are

$$A_1 = \begin{bmatrix} 0 & \frac{\langle \bar{q} \rangle_0 - 1}{L} \\ \frac{1 - \langle \bar{q} \rangle_0}{C} & -\frac{1}{RC} \end{bmatrix} \tag{27}$$

$$A_2 = \begin{bmatrix} 0 & \frac{2\langle \bar{q} \rangle_1^R}{L} & 0 & \frac{2\langle \bar{q} \rangle_1^I}{L} \\ 0 & \frac{-2\langle \bar{q} \rangle_1^R}{C} & 0 & \frac{-2\langle \bar{q} \rangle_1^I}{C} \end{bmatrix} \tag{28}$$

$$A_3 = \begin{bmatrix} 0 & \frac{\langle \bar{q} \rangle_1^R}{L} \\ \frac{-\langle \bar{q} \rangle_1^R}{C} & 0 \\ 0 & \frac{\langle \bar{q} \rangle_1^I}{L} \\ \frac{-\langle \bar{q} \rangle_1^I}{C} & 0 \end{bmatrix} \tag{29}$$

$$A_4 = \begin{bmatrix} 0 & \frac{\langle \bar{q} \rangle_0 - 1}{L} & \omega_s & 0 \\ \frac{1 - \langle \bar{q} \rangle_0}{C} & -\frac{1}{RC} & 0 & \omega_s \\ -\omega_s & 0 & 0 & \frac{\langle \bar{q} \rangle_0 - 1}{L} \\ 0 & -\omega_s & \frac{1 - \langle \bar{q} \rangle_0}{C} & -\frac{1}{RC} \end{bmatrix} \tag{30}$$

$$B_1 = \begin{bmatrix} \frac{\langle \bar{v} \rangle_0}{L} & \frac{2\langle \bar{v} \rangle_1^R}{L} & -\frac{2\langle \bar{v} \rangle_1^I}{L} \\ -\frac{\langle \bar{i} \rangle_0}{C} & \frac{-2\langle \bar{i} \rangle_1^R}{C} & \frac{2\langle \bar{i} \rangle_1^I}{L} \end{bmatrix} \tag{31}$$

$$B_2 = \begin{bmatrix} \frac{\langle \bar{v} \rangle_1^R}{L} & \frac{\langle \bar{v} \rangle_0}{L} & 0 \\ \frac{-\langle \bar{i} \rangle_1^R}{C} & \frac{\langle \bar{i} \rangle_0}{C} & 0 \\ \frac{\langle \bar{v} \rangle_1^I}{L} & 0 & -\frac{\langle \bar{v} \rangle_0}{L} \\ \frac{-\langle \bar{i} \rangle_1^I}{C} & 0 & -\frac{\langle \bar{i} \rangle_0}{C} \end{bmatrix}. \tag{32}$$

The system described in Equation (26) is a complete characterization of the multiharmonic small-signal model for the boost converter. The system diagram is shown in Figure 3, with an output matrix C that selects all voltage harmonic components as the outputs. Compared to the conventional small-signal model, which is a small-signal DC averaged model with a state matrix equal to A_1, the multiharmonic small-signal model provides more accurate circuit behavior by modeling the index-0 and index-1 components, as well as the interactions between them. This model can be easily extended to include harmonic components of an arbitrary degree.

4. SMALL-SIGNAL AC MODEL

In this section, we cast the proposed small-signal state-space model to the frequency domain to derive a linear time-varying AC model . We show how our AC model can immediately capture important high-frequency characteristics and lead to useful design insights.

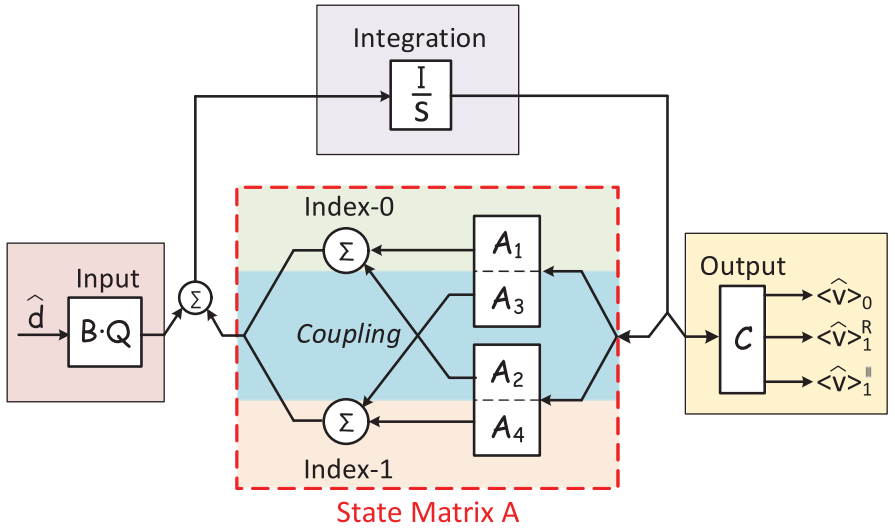

Fig. 3. The state space of the multiharmonic small-signal model and the interactions between its subsystems.

4.1. Frequency-Domain Small-Signal Model

The state-space model of Figure 3 outputs the index-0 and the real and imaginary parts of the index-1 components of the converter output voltage. These components can be combined to form the total voltage response:

$$\hat{v}(t) = \langle \hat{v} \rangle_0(t) + \langle \hat{v} \rangle_1(t) e^{j\omega_s t} + \langle \hat{v} \rangle_{-1}(t) e^{-j\omega_s t}, \tag{33}$$

where $v(t)$ is a combined output, and for convenience we have represented the index-1 component using complex exponentials. Applying the Laplace transform to Equation (33) gives the frequency-domain representation

$$\hat{v}(s) = \int_0^\infty \langle \hat{v} \rangle_0(t) e^{-st} dt + \int_0^\infty \langle \hat{v} \rangle_1(t) e^{(j\omega_s - s)t} dt + \int_0^\infty \langle \hat{v} \rangle_{-1}(t) e^{-(j\omega_s + s)t} dt, \tag{34}$$

which can be further simplified to

$$\hat{v}(s) = \langle \hat{v} \rangle_0(s) + \langle \hat{v} \rangle_1(s - j\omega_s) + \langle \hat{v} \rangle_{-1}(s + j\omega_s). \tag{35}$$

The small signal model of Equation (35) is a linear time-variant (LTV) system, which is illustrated in Figure 4. Each of $\langle \hat{v} \rangle_0$, $\langle \hat{v} \rangle_1$, and $\langle \hat{v} \rangle_{-1}$ can be characterized using a scalar LTI transfer function derived based on the small-signal state-space model. Note that the index-1 components $\langle \hat{v} \rangle_1(t)$ and $\langle \hat{v} \rangle_{-1}(t)$ are modulated by periodic signals $e^{j\omega_s t}$ and $e^{-j\omega_s t}$, which have frequency-shift effects in the frequency-domain response (Equation (35)).

4.2. Parametric Dependencies of High-Frequency Behavior

It is worth noticing that the proposed model captures the important high-frequency characteristics based on two mechanisms. First, as a model with six state variables, the proposed model accounts for high-frequency poles and zeros that are missing from traditional second-order models such as the ones presented in Erickson and Maksimovic [2007]. Second, the inclusion of the index-1 components takes into account additional high-frequency behaviors due to the frequency-shift effects.

Recall that the state matrix A from Equation (26) is a 6×6 matrix that has four submatrices, where A_1 and A_4 correspond to the subsystem of the index-0 and index-1

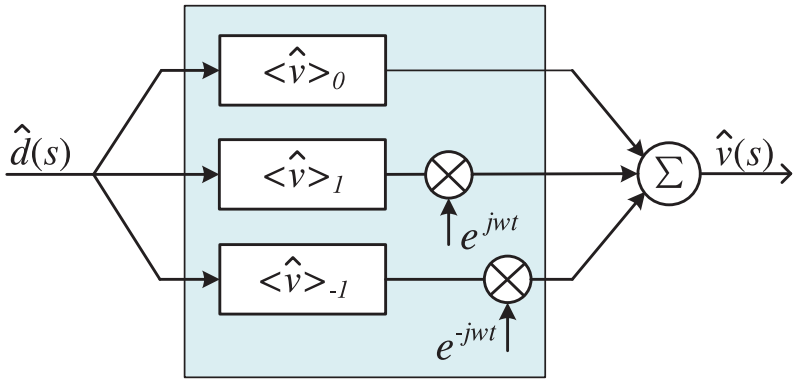

Fig. 4. Illustration of the linear time-variant (LTV) system with the frequency-shift effect.

harmonic components. As pointed out in Pérez-Arriaga et al. [1990], there is a distinctive model separation in system A and we can closely approximate the eigenvalues of A using those of the submatrices A_1 and A_4. From Equation (30), we evaluate the eigenvalues of A_4 analytically [Caliskan et al. 1999]:

$$\lambda_{1,2}(A_4) = -\alpha \pm j\left(-\omega_s + \sqrt{{\omega_n}^2 - \alpha^2}\right) \tag{36}$$

$$\lambda_{3,4}(A_4) = -\alpha \pm j\left(\omega_s + \sqrt{{\omega_n}^2 - \alpha^2}\right), \tag{37}$$

where $\omega_n = \frac{1-d}{\sqrt{LC}}$, $\alpha = \frac{1}{2R_LC}$, and ω_s is the switching frequency of the converter. In our case, system eigenvalues are actually the poles for the corresponding transfer functions. For each pair of complex conjugates we derive the quality factor Q, which indicates the magnitude of the resonant overshoot, and the angular corner frequency ω_0, which indicates the location of the corresponding overshoot. For boost converters, we have

$$\begin{aligned} Q &= \frac{1}{2\alpha}\sqrt{\alpha^2 + \left(\omega_s \pm \sqrt{{\omega_n}^2 - \alpha^2}\right)^2} \\ &\approx \frac{1}{2\alpha} \cdot |\omega_s \pm \omega_n| \end{aligned} \tag{38}$$

and

$$\begin{aligned} \omega_0 &= \sqrt{\alpha^2 + \left(\omega_s \pm \sqrt{{\omega_n}^2 - \alpha^2}\right)^2} \\ &\approx |\omega_s \pm \omega_n|. \end{aligned} \tag{39}$$

The effects of Q and ω_0 on resonant overshoot are illustrated in Figure 5. From Equation (39), it is clear that the overshoots appear around the switching frequency ω_s, and hence have a significant effect on the converter's high-frequency response. For converter systems with Q larger than 1, there will be large overshoots/spikes around the switching frequency, which can potentially lead to stability problems. In the following converter design examples, we will show how high-frequency overshoots eventually lead to instability of the closed-loop system and how this can be fixed by adjusting the converter design parameter to reduce the value of Q.

5. EXPERIMENTAL RESULTS

We demonstrate the application of the proposed model using two different converter examples. The two converter types selected are the boost converter shown in Figure 1

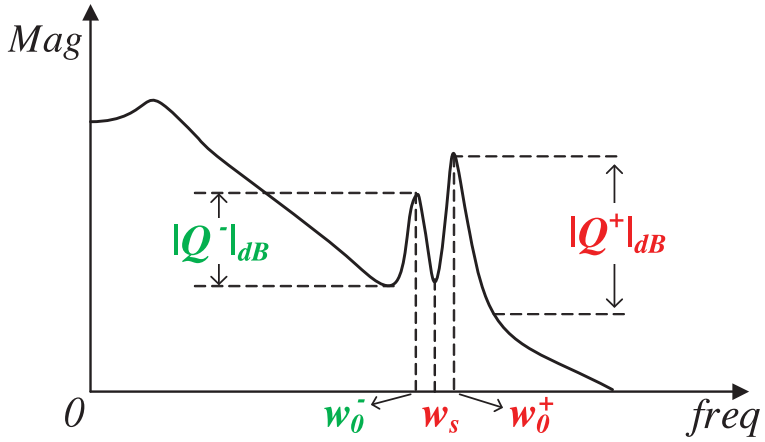

Fig. 5. The effect of Q and ω_0 on a boost converter frequency response.

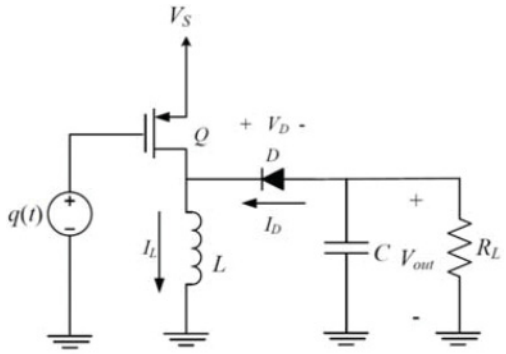

Fig. 6. The buck-boost converter.

Table I. Circuit Parameters

	$R[\Omega]$	$C[F)]$	$L[H]$	$f_s[Hz]$	$V_{in}[V]$	d [ratio]
Boost converter	20	50μ	75μ	100k	2	0.4
Buck-boost converter	4	220μ	50μ	10k	4	0.4

and the buck-boost converter shown in Figure 6. The nominal duty ratio for both converters is 0.4 with the full set of parameters for both converter types, as shown in Table I. We analyze the frequency response of each converter circuit using the proposed small-signal model and compare the results with the frequency response obtained using the conventional small-signal model, which is based on the average model that only considers the DC component of the Fourier series of the signals [Erickson and Maksimovic 2007]. We also compared our proposed model with some reference values, which are the actual gain values obtained from a transient analysis. These reference values were calculated by first perturbing the duty ratio by a small amount (0.001 or 0.1% in both cases) and then measuring the resulting perturbation of the average of the output voltage. The perturbation is a sinusoidal waveform, and the commercial tool used for performing the transient analysis is Cadence Virtuoso. Finally, we demonstrate how the conventional small-signal model can lead to a false understanding of the

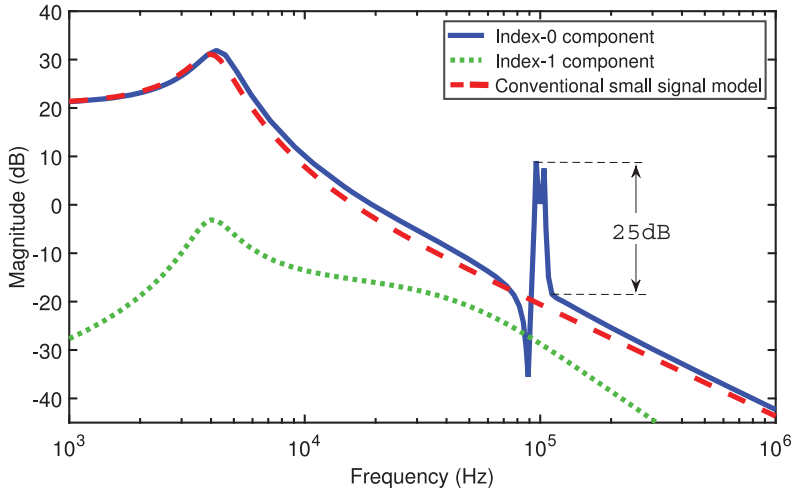

(a) Example 1: boost converter

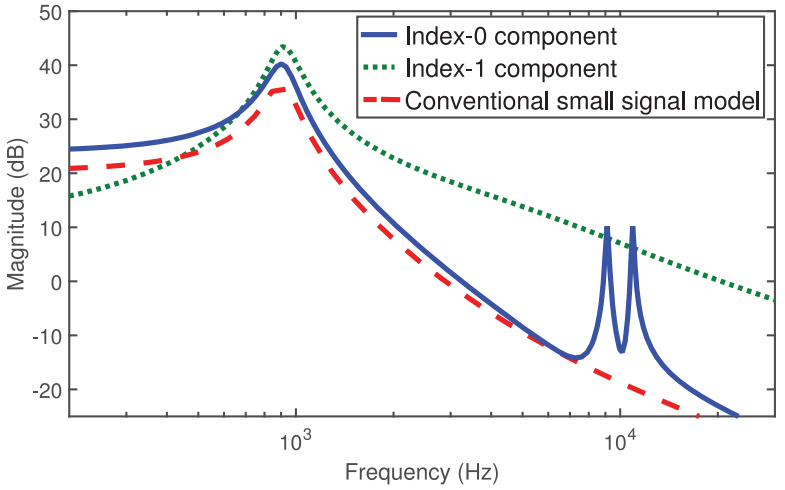

(b) Example 2: buck-boost converter

Fig. 7. The control-to-output transfer functions of the DC-DC converters modeled by the proposed small-signal model (index-0 and index-1) and the conventional small-signal model.

closed-loop stability and how our proposed model can aid in the compensator design to ensure stability of the two converters.

5.1. Analysis of the Frequency-Domain Responses

Figure 7 shows the index-0 and index-1 harmonic components of each converter obtained by the proposed small-signal model. Compared with the transfer function obtained by the conventional small-signal model, our proposed model demonstrates enhanced accuracy and reveals important response characteristics and design insights. Figure 8 also shows a direct comparison with the ground-truth reference values. As can be seen, the proposed method again demonstrates significantly improved accuracy relative to the reference values when compared with the traditional model.

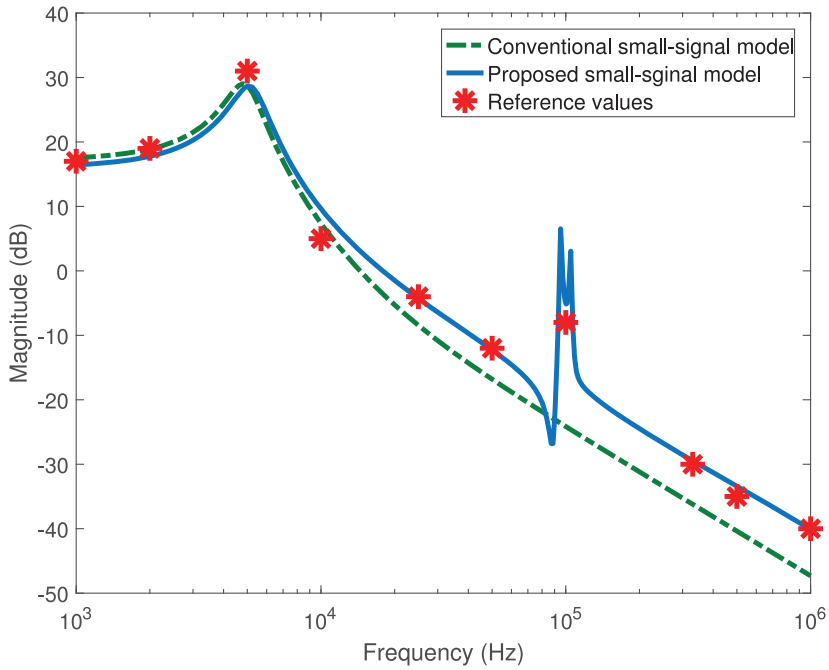

(a) Example 1: boost converter

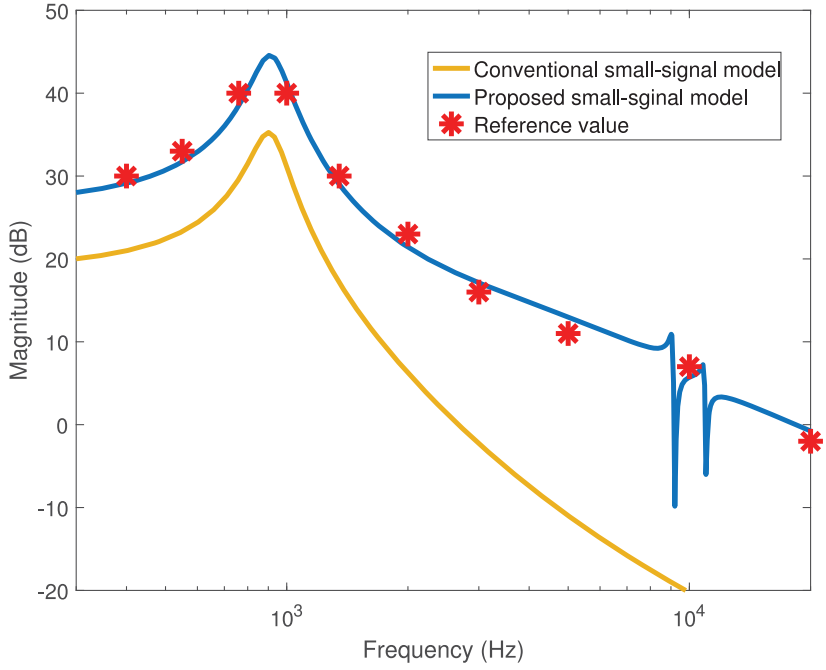

(b) Example 2: buck-boost converter

Fig. 8. Comparison of our proposed model, traditional small signal model, and reference values.

Table II. Lead Compensator Designs Based on the Conventional Small-Signal Model and the Proposed Small-Signal Model

	Conventional Small-Signal Model	Proposed Small-Signal Model
Boost converter	$\frac{2.61s+1.47\times10^4}{s+3.85\times10^4}$	$\frac{4.22s+1.22\times10^5}{s+5.17\times10^5}$
Buck-boost converter	$\frac{4.41s+1.02\times10^5}{s+4.53\times10^5}$	$\frac{42.3s+2.73\times10^4}{s+1.16\times10^4}$

The first converter we analyzed is the boost converter, with the resulting plots as shown in Figure 7(a) and Figure 8(a). The index-1 component is negligible in this example. Because our proposed model is a six-state model that also captures the index-0 and index-1 interactions, the computed index-0 component captures several spikes around the switching frequency. The peak magnitude of the spikes is $25dB$, which means that the switching noise is essentially amplified by the boost converter. As we will show later in the closed-loop simulation, the amplified switching noise affects the stability of the system by disrupting the behavior of the pulse-width modulator [Erickson and Maksimovic 2007]. On the other hand, the conventional small-signal model only demonstrates a typical two-pole low-pass filter characteristic, without showing any sign of high-frequency spikes or instability.

The second example converter we analyzed is the buck-boost converter, with the resulting plots as shown in Figure 7(b) and in Figure 8(b). The frequency responses obtained by the proposed small-signal model shows that the index-0 component has a large low-frequency gain with two spikes around the switching frequency. The index-1 harmonic component has a significant magnitude at high frequency, which indicates that the harmonic component of the converter response is sensitive to the perturbation of the duty ratio. On the other hand, the conventional small-signal model only captures behavior of the index-0 component, which provides no information on the harmonics of the response. As will be shown next in the compensator design example, large harmonic components can possibly lead to an unstable closed-loop design.

5.2. Stability Analysis and Closed-Loop Design

For each converter circuit, we design a lead compensator based on the gain crossover frequency and the open-loop phase margin obtained from the frequency response of the conventional small-signal model, which is based on the average model that only considers the DC component of the Fourier series of the signals [Erickson and Maksimovic 2007]. Table II shows the lead compensator transfer functions for both converters. Figure 9 shows the transient simulation of the closed-loop systems using the converters and the designed compensators. It is clear that the compensators based on the conventional small-signal model fail to stabilize either converter circuit in the start-up transient simulation.

The failure of the compensator design demonstrates the limitation of the conventional small-signal model in modeling the high-frequency behavior of DC-DC converters. On the other hand, our proposed model can accurately capture high-frequency circuit behaviors and provide truthful responses since it is based on a multiharmonic averaged model, which considers the DC component, the first-order component, and the interactions between them. In fact, the index-0 component of the proposed model predicts the instability of the previously designed closed-loop systems. According to the revised bode stability criterion [Hahn et al. 2001], both compensated systems are unstable with negative gain margins of $-15dB$ and $-11dB$.

Taking things a step further, we will use the proposed model to improve the closed-loop design and correct the compensator designs, which eventually regains the stability of the closed-loop systems. In the first example, the causes of the instability of the boost converter are the spikes around the switching frequency. As discussed in Section 4.2,

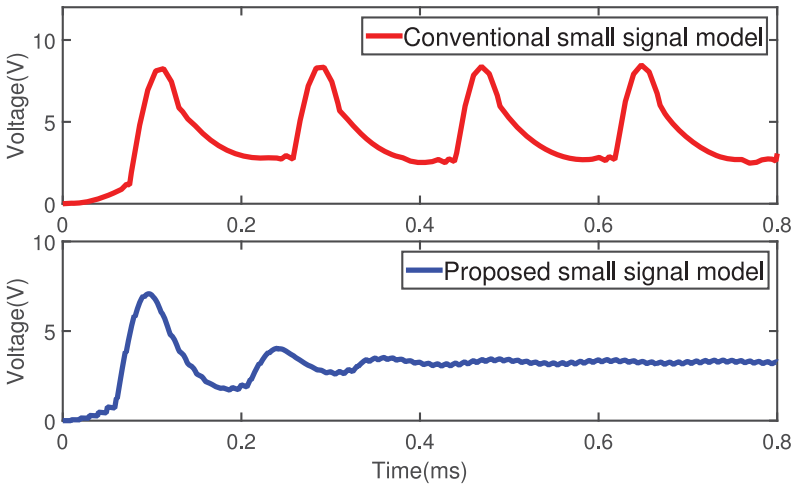

(a) Example 1: boost converter

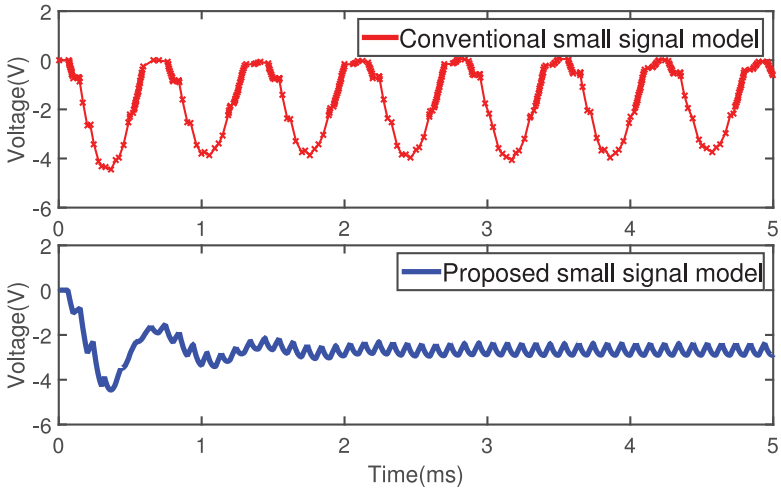

(b) Example 2: buck-boost converter

Fig. 9. Comparison of the transient responses of the closed-loop systems designed by the conventional small-signal model and the proposed small-signal model.

these spikes are essentially high-frequency overshoots of the index-0 component. To reduce the magnitude of the spikes, we reduce the quality factors. According to Equation (38), the maximum quality factor of the boost converter is $Q = 26.3 = 28dB$, which is a good estimation of the amplitude of the spike shown in Figure 7(a). By changing the value of the output capacitance C from $50\mu F$ to $10\mu F$, the value of the quality factor is reduced to 1.5 and the magnitude of the spike is reduced to $2.3dB$, which is less than 8% of the original spike magnitude. Then, we design a new lead compensator using the frequency response of the improved converter design. As shown by the transient simulation in Figure 9(a), the closed-loop system becomes stable.

In the second example, the conventional small-signal model, which is a simple second-order model, fails to reveal the potential design problems due to the large magnitude

of the index-1 component. To properly design a stable closed-loop system, we suppress the amplitude of the index-1 component. By adjusting the converter parameters to $L = 800\mu H$ and $C = 10\mu F$, we are able to limit the maximum magnitude of the index-1 component in all frequencies under $2dB$. With the new converter design, we redesign the lead compensator based on the gain crossover frequency obtained from our index-0 model. The transfer function of the lead compensator is shown in Table II. With the new lead compensator, the output voltage of the buck-boost converter settles down as shown in Figure 9(b), which validates the stability of the closed-loop system.

6. CONCLUSION

In this article, a novel multiharmonic small-signal model that accurately accounts for the high-frequency responses of the DC-DC converters is presented. Compared with existing small-signal models, the proposed model considers both the DC averages and the higher-order harmonic components in addition to the interactions between them, thereby providing a complete small-signal characterization of the converter circuits. Two converter design examples are presented, which demonstrate the significant improvements of the proposed model on frequency-domain response analysis, stability analysis, and closed-loop design.

REFERENCES

V. A. Caliskan, O. C. Verghese, and A. M. Stankovic. 1999. Multifrequency averaging of DC/DC converters. *IEEE Transactions on Power Electronics* 14, 1 (1999), 124–133.

R. W. Erickson and D. Maksimovic. 2007. *Fundamentals of Power Electronics*. Springer Science & Business Media.

P. Feldmann and J. Roychowdhury. 1996. Computation of circuit waveform envelopes using an efficient, matrix-decomposed harmonic balance algorithm. In *Proceedings of the International Conference on Computer Aided Design*. 295–300.

J. Groves. 1991. Small-signal analysis using harmonic balance methods. In *Proceedings of the 1991 IEEE Power Electronics Specialists Conference*. IEEE.

J. Hahn, T. Edison, and T. F. Edgar. 2001. A note on stability analysis using bode plots. In *Chemical Engineering Education*. 208–211.

J. M. Noworolski and S. R. Sanders. 1991. Generalized in-plane circuit averaging. In *Proceedings of the 6th Annual Applied Power Electronics Conference and Exposition, 1991 (APEC'91)*. IEEE, 445–451.

I. J. Pérez-Arriaga, G. C. Verghese, F. L. Pagola, J. L. Sancha, and F. C. Schweppe. 1990. Developments in selective modal analysis of small-signal stability in electric power systems. *Automatica* 26, 2 (1990), 215–231.

Y. Qiu, M. Xu, K. Yao, J. Sun, and F. C. Lee. 2006. Multifrequency small-signal model for buck and multiphase buck converters. *IEEE Transactions on Power Electronics* 21, 5 (2006), 1185–1192.

S. R. Sanders, J. M. Noworolski, X. Z. Liu, and G. C. Verghese. 1991. Generalized averaging method for power conversion circuits. *IEEE Transactions on Power Electronics* 6, 2 (1991), 251–259.

L. Scandola, L. Corradini, and G. Spiazzi. 2015. Multi-harmonic small-signal modeling of digitally controlled dc-dc series resonant converters. In *IEEE Workshop on Control and Modeling for Power Electronics (COMPEL'15)*. IEEE, 1–8.

D. Shortt and F. Lee. 1982. An improved switching converter model using discrete and average techniques. In *1982 IEEE Power Electronics Specialists conference*. IEEE, 199–212.

J. Sun, D. M. Mitchell, M. F. Greuel, P. T. Krein, and R. M. Bass. 2001. Averaged modeling of PWM converters operating in discontinuous conduction mode. *IEEE Transactions on Power Electronics* 16, 4 (2001), 482–492.

D. Tannir, Y. Wang, and P. Li. 2016. Accurate modeling of nonideal low-power PWM DC-DC converters operating in CCM and DCM using enhanced circuit averaging techniques. *ACM Transactions on Design Automation of Electronic Systems* 21, 4 (2016), 1–15.

G. C. Verghese, M. E. Elbuluk, and J. G. Kassakian. 1986. A general approach to sampled-data modeling for power electronic circuits. *IEEE Transactions on Power Electronics* 2 (1986), 76–89.

V. Vorperian. 1990. Simplified analysis of PWM converters using model of PWM switch. Continuous conduction mode. *IEEE Transactions on Aerospace Electronic Systems* 26, 3 (May 1990), 490–496. DOI:http://dx.doi.org/10.1109/7.106126

V. Vorpérian. 1990. Simplified analysis of PWM converters using model of PWM switch. II. Discontinuous conduction mode. *IEEE Transactions on Aerospace Electronic Systems* 26, 3 (1990), 497–505.

Y. Wang, D. Gao, D. Tannir, and P. Li. 2016. Multi-harmonic nonlinear modeling of low-power PWM DC-DC converters operating in CCM and DCM. In *Proceedings of the 2016 Design, Automation & Test in Europe Conference & Exhibition*. EDA Consortium.

G. W. Wester and R. D. Middlebrook. 1973. Low-frequency characterization of switched dc-dc converters. *IEEE Transactions on Aerospace Electronic Systems* 3 (1973), 376–385.

Z. Zeng, S. Lai, and P. Li. 2013. IC power delivery: Voltage regulation and conversion, system-level cooptimization and technology implications. *ACM Transactions on Design Automation of Electronic Systems* 18, 2 (2013), 1–15.

Received September 2016; revised January 2017; accepted February 2017